Deformable Prostate Registration from MR and TRUS Images Using Surface Error Driven FEM models

Farheen Taquee[a], Orcun Goksel[b], S. Sara Mahdavi[a], Mira Keyes[c], W. James Morris[c], Ingrid Spadinger[c], Septimiu Salcudean[a]

[a]University of British Columbia, 2332 West Mall, Vancouver, British Columbia, Canada;
[b]ETH, Computer Vision Lab, Sternwartstr 7, 8092, Zürich, Switzerland;
[c]BC Cancer Agency, 600 10th Ave W, Vancouver, British Columbia, Canada

ABSTRACT

The fusion of TransRectal Ultrasound (TRUS) and Magnetic Resonance (MR) images of the prostate can aid diagnosis and treatment planning for prostate cancer. Surface segmentations of the prostate are available in both modalities. Our goal is to develop a 3D deformable registration method based on these segmentations and a biomechanical model. The segmented source volume is meshed and a linear finite element model is created for it. This volume is deformed to the target image volume by applying surface forces computed by assuming a negative relative pressure between the non-overlapping regions of the volumes and the overlapping ones. This pressure drives the model to increase the volume overlap until the surfaces are aligned. We tested our algorithm on prostate surfaces extracted from post-operative MR and TRUS images for 14 patients, using a model with elasticity parameters in the range reported in the literature for the prostate. We used three evaluation metrics for validating our technique: the Dice Similarity Coefficient (DSC) (ideally equal to 1.0), which is a measure of volume alignment, the volume change in source surface during registration, which is a measure of volume preservation, and the distance between the urethras to assess the anatomical correctness of the method. We obtained a DSC of 0.96±0.02 and a mean distance between the urethras of 1.5±1.4 mm. The change in the volume of the source surface was 1.5±1.4%. Our results show that this method is a promising tool for physically-based deformable surface registration.

Keywords: Deformable, Registration, Prostate, Finite Element, Magnetic Resonance, Transrectal Ultrasound

1. INTRODUCTION

Integrating TransRectal UltraSound (TRUS) and Magnetic Resonance (MR) images of prostate can be useful for biopsy guidance,[1] treatment planning (brachytherapy,[2] focal therapy[3]) and surgery.[4] It also has applications in long term quality assurance for brachytherapy. There is extensive literature available on the general subject; however, prior work in the specific category of TRUS to MR prostate image registration is limited.

Due to different patient positions, bladder fullness and the presence of the TRUS probe in the rectum, pre-operative and intra-operative TRUS images cannot be accurately registered rigidly;[5] non-rigid registration methods are thus required. In terms of inputs and processing domains, such methods can be classified in two categories, intensity-based and surface-based.

Several surface based models for MR and TRUS prostate registration have been proposed. Thin plate splines,[6,7] polynomials[8] and dynamic finite-element surface-spine models[9] have been used to warp prostate surfaces. Other approaches include minimizing the Haussdorf distance between a surface and a point cloud[2] and the use of a biomechanical model.[10] The latter used a linearly-elastic finite element model with different material properties for the central and peripheral zones of the prostate driven by surface distance based forces. Non-linear elastic models have also been utilized to perform MR to MR prostate registration.[11] More recently,

Further author information:
Septimiu Salcudean, tims@ece.ubc.ca, Tel. 1 (604) 822-3243.

Medical Imaging 2012: Image-Guided Procedures, Robotic Interventions, and Modeling,
edited by David R. Holmes III, Kenneth H. Wong, Proc. of SPIE Vol. 8316, 831612

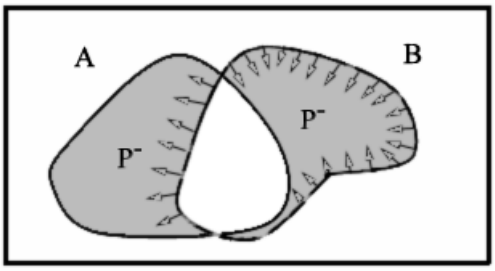

Figure 1: Overlapping and non-overlapping regions are shown in white and gray colors respectively. Consider A as the target surface and B as the source. The forces produced as the result of the negative pressure (P^-) in the gray regions are shown by the arrows.

patient specific finite element statistical models[12] have been used to perform deformable registration between MR and TRUS postate surfaces.

We propose a surface based registration method to deformably register segmented contours using a biomechanical model. The model is a linear elastic body which deforms when subjected to external forces on its surface. Similar models have been previously used to perform deformable registration.[10,12–14] The main difference between the registration approach presented in this paper and the ones presented in the past is the nature of external forces driving the deformable model. Here we employ forces based on the global surface difference instead of local surface differences (distances) and therefore produce a more realistic distribution of forces driving the model to the target. Furthermore, the approach in this paper has been validated with elasticity parameters typical of those reported in the literature, and not based on the quality of the registration surface match. This emphasizes the importance of the deformable physical model and its realistic parametrization, rather than simply using it as a spatial smoother for the regularization of registration. The results are evaluated in terms of the improvement achieved in the matching of the prostate volumes. In addition, the distances between the urethra segmentations in the two modalities are used as an independent measure of registration accuracy.

2. METHOD

We perform an initial course registration by first aligning the centers of mass and then the principle axes (the base-apex axes) of the two surfaces. We create a linear elastic finite element model of the volume enclosed by one of the surfaces, called the *source surface*. We call the other surface the *target surface*. The intersection and union surfaces of the source and target surfaces are created to find the overlapping and non-overlapping regions. The forces used to deform the source surface are caused by an assumed negative pressure in the overlapping volume. An illustration of the presence of this pressure and the resulting force on the source surface can be seen in Figure 1. This pressure pulls the non-overlapped region of the source surface towards the target surface and pulls the overlapped volume of the source surface towards the interior of the target surface in order to maximize the overlapped volume between the source and target surfaces. The goal of the registration in this context becomes to minimize the non-overlapped volume and which in turn maximizes the overlapped volume. The overview of our algorithm can be found in Figure 2, where the stopping criterion is reaching a minimum of the non-overlapping volume.

We use the standard finite element method to simulate elastic solids with tetrahedral elements. The solid is discretized into a number of finite elements in the form of tetrahedrons and nodes. The force of an element f^e resulting from a displacement of nodes u^e is given by $f^e = K^e u^e$ where K^e, the stiffness matrix of an element, is a function of the volume and the shape of the tetrahedron and of its material properties. A global stiffness $\mathbf{K}$ is then assembled from these element matrices leading to the following sparse linear system:

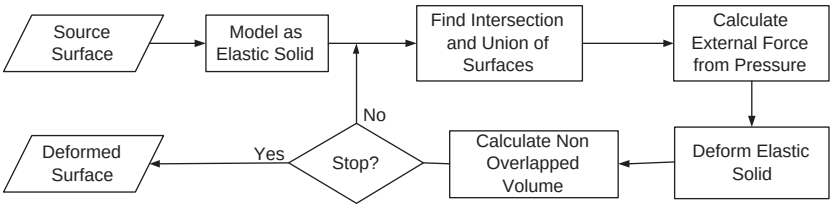

Figure 2: Block diagram showing the deformable registration algorithm

$$\mathbf{Ku} = \mathbf{F} \tag{1}$$

where $\mathbf{F}$ is an array of forces on all the nodes and $\mathbf{u}$ is the deformation field of the entire mesh.[15] We used the following semi-implicit equation used by Ferrant et al.[16] for time discretization of our dynamic FEM model:

$$(\mathbf{I} + \tau\mathbf{K})\mathbf{u}^t = \mathbf{u}^{t-1} + \tau\mathbf{F}(\mathbf{u}^{t-1}) \tag{2}$$

where $\mathbf{u}^t$ is the array of nodal displacements at iteration t, $\mathbf{F}(\mathbf{u}^{t-1})$ is the driving force calculated at iteration $t-1$ and τ is the time step.

As illustrated in Figure 1, if we have two surfaces A and B with volumes V_A and V_B which partially overlap each other, an intersection surface with volume $V_{A\cap B}$ and a union surface with the volume $V_{A\cup B}$ can be created. The Dice Similarity Coefficient (DSC) for the volumes can be calculated as:

$$DSC(A,B) = \frac{2 \times V_{A\cup B}}{V_A + V_B} \tag{3}$$

Two perfectly registered surfaces should have a DSC of 1.

After every iteration t, the union and intersection surfaces are created and the non-overlapping volume is calculated. The driving force for each mesh node is calculated from the negative pressure in this non-overlapping volume. This pressure will only affect the source surface as we assume that the target surface cannot move. It is applied uniformly on the source surface which then produces forces on a triangular surface element equal to the pressure times the area of that element. The direction of this force is normal to the plane of the triangle. It can be pointing inwards or outwards of the source surface, depending on whether the node is part of the union or the intersection of the surfaces, respectively. This force is divided equally to the nodes that form that triangle.

Mathematically, if $\mathbf{n}(\mathbf{f})$ is a vector representing the face normal of a triangular face '$\mathbf{f}$' in the outward direction to the surface, and $A(\mathbf{f})$ is the area of the face and P is the pressure, then the force on the face $F_t(f)$ is given by:

$$F_t(f) = D \times A(f) \times P \times \mathbf{n}(\mathbf{f}) \tag{4}$$

The direction D is determined by :

$$D = \begin{cases} +1 \text{ if } t \in S_{int} \\ -1 \text{ if } t \in S_{uni} \end{cases}$$

where S_{int} is intersection surface and S_{uni} is union surface.

Every node receives the contribution of forces from the connected elements and the resultant is computed. See Figure 3 for an illustration. If a node p is surrounded by n faces then:

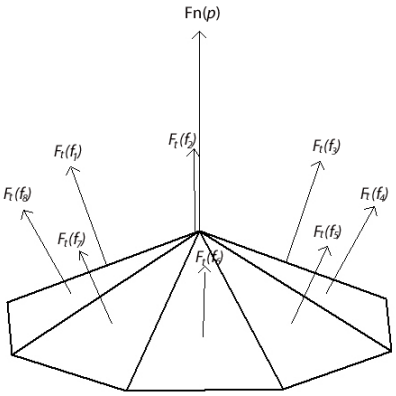

Figure 3: A number of connected surface triangles. The tetrahedral structure is ignored for ease of visualization. The pressure results in force on a triangular face with direction normal to it ($F_t(f_n)$, where n=8). The force at the node ($\mathbf{Fn}(p)$) connected to all these faces is the sum of these forces.

$$\mathbf{Fn}(p) = \sum_n \frac{1}{3} \times F_t(f_n) \tag{5}$$

The vector of nodal forces can be formed from (5) such that:

$$\mathbf{F} = [\, fnx_1, fny_1, fnz_1, ..., fnx_m, fny_m, fnz_m \,]^T \tag{6}$$

where m is the total number of nodes and fnx, fny and fnz are x, y and z components of $\mathbf{Fn}$. Figure 4 shows distribution of nodal forces in a mesh.

During the registration process, as the source and target surfaces become close to each other, chattering of forces can be observed as the surfaces cross over and the forces change directions abruptly. Low pass filtering of the forces produces sufficient averaging to insure oscillation-free convergence of our dynamic model. The non-overlapping volume decreases with time during the registration unless the time step is too large. Therefore the algorithm decreases the time step by half whenever the non-overlapping volume increases. The algorithm stops when the change in overlapping volume is less than a prespecified value. This indicates that the surface has stopped deforming and the algorithm has converged.

3. EVALUATION AND RESULTS

We applied our registration method to 14 pairs of prostate surfaces obtained from post-operative TRUS and MR images. These images had the prostate boundary and the urethras segmented. We used Stradwin[17] to obtain the triangulated surfaces from these contours. The US surfaces were meshed using TetGen[18] to obtain tetrahedral mesh elements. CGAL[19] was used to create the intersection and union surfaces. We have used a Youngs Modulus of 10KPa (a value based on the average Shear Modulus reported in the peripheral zone of the prostate[20]) and a Poisson's ratio of 0.49 to calculate the stiffness matrix $\mathbf{K}$. The non-overlapping volume is penalized by a pressure of 1KPa which is set such that the resulting force on the mesh is of the order of 10^{-1} N which is in the same order of magnitude as the gravitational force on the prostate. The MR surface was used as the target surface and the TRUS surface was used as the source surface.

We have used three criteria for evaluation of this method. The first is the DSC which shows how well-registered the two surfaces are in terms of volume overlap. The second is the volume difference between the source and target surfaces. There is always a difference in the surface volume of the surfaces extracted from the contours of the same organ in different modalities due to segmentation errors and mesh discretization errors.

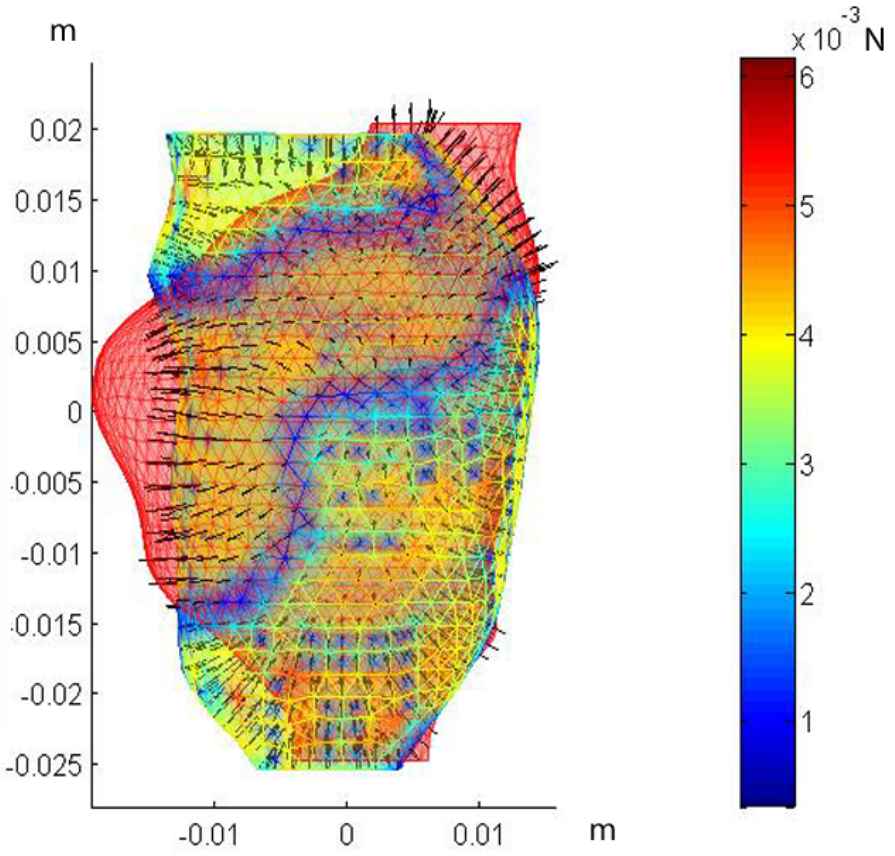

Figure 4: Force distribution in a mesh from real patient data. The mesh is color-coded with the magnitude of nodal forces. The direction of forces can be seen from the arrows originating from the surface node of the mesh.

We calculated the volume difference between the target and the source, normalized it by the source volume, and present this as a percentage.

A positive volume difference indicates a higher volume enclosed by the target surface. Ideally, this volume difference should remain the same after registration if the volume is preserved. Another important measure of evaluation of the registration is provided by computing a target registration error (TRE) using landmarks. As there are no fiducials or landmarks visible in the TRUS and MR images, we use the urethra as a landmark as its clearly visible in most of the MR images, and also in the TRUS images, due to the presence of a Foley catheter.

The DSC using equation (3), volume difference and distance between the urethras in the two imaging modalities were calculated before and after the registration. Splines were fitted through the centers of segmented contours of the urethra cross-sections in order to represent urethra center-line. The maximum and mean distance between the source and target urethra center-lines is measured before the deformable registration. After the registration, the coordinates of the urethra contours in the deformed mesh are calculated using the basis functions of the tetrahedra in which they lie. This gives the center-line of the urethra in the deformed mesh which we then use to compute a post-registration TRE. Figure 5 shows the unregistered and registered meshes with splines showing the urethra center-lines. The mean distance between the urethra in the deformed TRUS and the urethra in the MR urethra was computed for each patient.

We performed registration of 14 pairs of post-operative MR-US prostate surfaces with and without initial principal axis alignment (PAA) to test sensitivity of our algorithm to initial alignment. Table 1 presents the

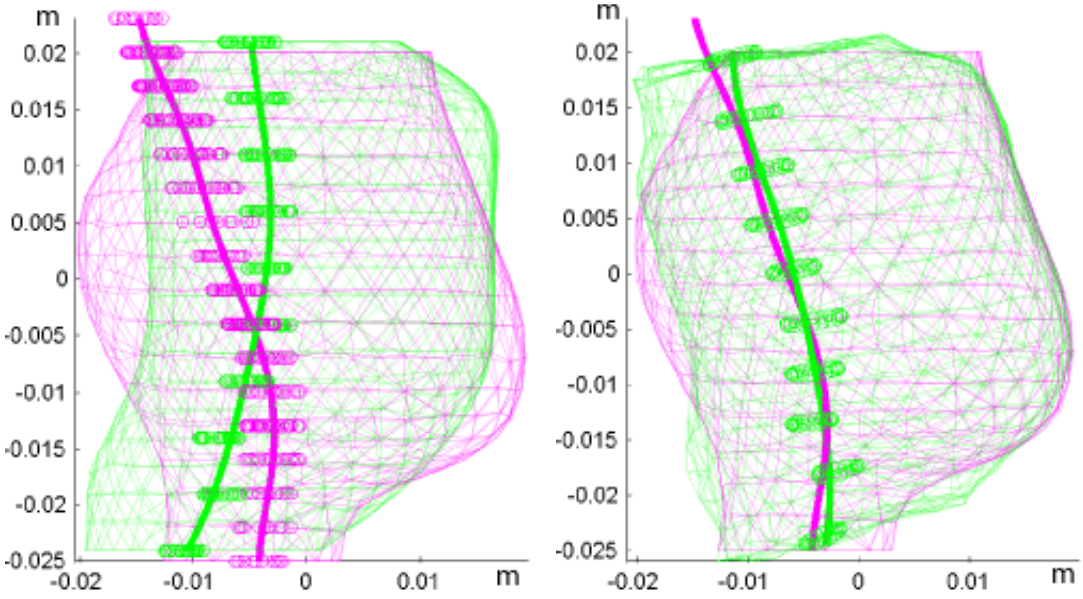

(a) Before Deformable registration (b) After Deformable registration

Figure 5: Results of our deformable registration for Case 5. The pink and green meshes represents the target and the source surfaces respectively. The urethras from both the volumes are shown by the fitted splines of the corresponding colours. The MR surface was used as the target surface and the TRUS surface was used as the source surface.

results of this evaluation. The volume difference (VD), the DSC and the TRE (maximum and mean ± standard deviation of the distance between urethras) are reported.

4. DISCUSSION AND CONCLUSION

In this paper we presented a new method of using linear elastic models to register MR to TRUS images. It can be seen from Table 1 that both the DSC and the distance between the urethras were reduced for most of the cases. The mean DSC for the 14 patients was 0.96±0.02 when PAA was not used and 0.95±0.02 when PAA was used. Figure 6 shows the DSC values before and after registration. The presence of segmentation error and difference in volumes between the fixed and source surfaces is accountable for the lower DSC.

The volume difference, which is used to ensure that the volume is preserved, changes insignificantly (less than 6%) in all cases which can be attributed to the differences in volumes of the source and target surfaces. For the 14 cases, the mean change in volume difference was 1.5±1.4% when PAA was used and 1.9±1.4% when PAA was not used.

The mean TRE for 14 cases was 1.5±1.4 mm when PAA was not used and 1.6±1.4 mm when PAA was used. The maximum TRE decreased after registration in 12 out of 14 cases. A bar graph showing maximum TRE before and after registration is presented in figure 6. The mean TRE increased by more than 0.1 mm in three cases. In these three cases, the higher distance between the urethras can be attributed to the lower visibility of the urethra and prostate boundary in the noisy post-brachytherapy US images. The prostate boundary is usually not well defined in the post-brachytherapy US images and it is difficult to visualize the prostate and the urethra at the prostate base and apex. Please also note that in case 9, although the mean distance increased, the standard deviation decreased significantly (see figure 7). Figure 8 (b) shows the registered meshes for case 9 using our approach.

The urethra has been used for the evaluation of the registration between TRUS and MR images by Reynier et al.[2] and Porter et al.[21] In the former, the mean distance between the urethras is as high as 5 mm near the

Case	VD(%)	PAA	DSC		TRE Before (mm)		TRE After (mm)		VC(%)
			Before	After	Mean	Max	Mean	Max	
1	2.7	No	0.81	0.95	0.8±0.5	2.7	0.7±0.5	1.9	1.4
		Yes	0.81	0.95	1.6±1.4	4.9	0.8±0.6	1.9	2.0
2	2.5	No	0.89	0.95	1.0±0.7	2.6	1.7±1.4	4.5	0.0
		Yes	0.89	0.95	1.0±0.7	2.6	1.8±1.5	4.8	0.5
3	0.8	No	0.89	0.94	0.7±0.5	1.7	0.9±0.8	2.6	2.4
		Yes	0.89	0.94	0.7±0.5	1.7	0.9±0.8	2.6	2.5
4	2.7	No	0.94	0.98	1.1±0.9	3.0	0.9±0.8	2.9	1.2
		Yes	0.93	0.98	1.4±1.2	3.4	0.8±0.9	2.9	2.3
5	3.2	No	0.85	0.95	2.3±1.6	6.4	0.7±0.6	2.0	3.7
		Yes	0.88	0.94	0.7±0.5	2.2	0.5±0.4	1.6	-0.9
6	3.8	No	0.92	0.96	1.3±0.9	3.0	0.5±0.4	1.8	-0.3
		Yes	0.92	0.96	1.2±0.8	3.4	0.6±0.5	2.3	-0.3
7	1.9	No	0.92	0.98	4.4±2.4	7.7	3.8±1.0	5.5	2.3
		Yes	0.93	0.97	4.5±1.5	6.3	3.7±1.0	5.2	1.5
8	2.6	No	0.81	0.91	2.9±2.3	8.8	1.0±1.1	4.4	1.2
		Yes	0.80	0.91	2.0±2.4	7.6	1.2±1.2	5.0	4.6
9	4.8	No	0.86	0.95	1.9±1.5	4.7	3.0±0.4	3.9	4.8
		Yes	0.86	0.94	3.5±1.9	7.5	3.5±0.7	4.7	5.7
10	-2.1	No	0.90	0.96	0.9±0.7	2.5	1.1±0.7	2.0	-1.2
		Yes	0.90	0.96	0.9±0.7	2.5	1.0±0.6	1.9	-1.2
11	-2.6	No	0.88	0.96	1.6±0.9	3.4	1.4±0.8	2.9	-0.2
		Yes	0.85	0.95	2.6±1.7	6.0	1.8±1.0	3.7	3.4
12	-4.1	No	0.94	0.97	1.6±1.0	4.4	1.7±0.7	3.4	-0.3
		Yes	0.93	0.96	2.6±1.2	4.9	1.9±1.0	4.2	0.3
13	2.6	No	0.93	0.97	2.3±1.2	3.7	1.3±0.7	2.1	-0.3
		Yes	0.94	0.98	1.9±0.9	3.0	1.6±0.8	2.6	1.1
14	-4.4	No	0.91	0.96	2.9±2.2	6.6	3.0±2.1	6.3	0.4
		Yes	0.91	0.95	3.3±2.4	7.4	2.9±2.1	6.2	1.0

Table 1: Results for the fourteen post brachytherapy images showing the DSC and TRE measures before and after registration when principle axis alignment(PAA) was and was not performed. The volume change (VC) in surface after registration and volume difference (VD) between the source and target surface is also reported.

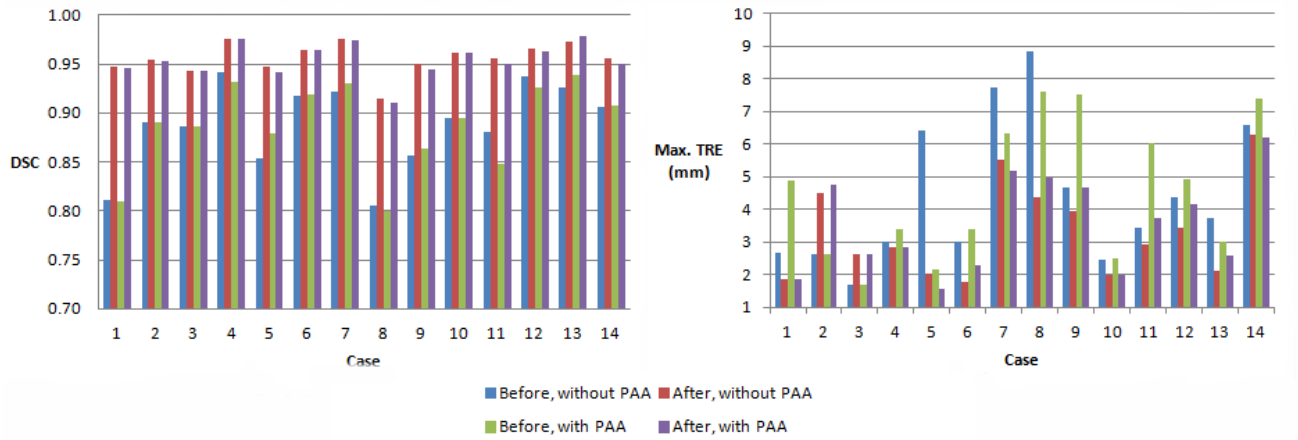

Figure 6: Dice similarity coefficient and maximum target registration error values for the fourteen cases before and after deformable registration. The values with and without initial principal axis alignment are depicted.

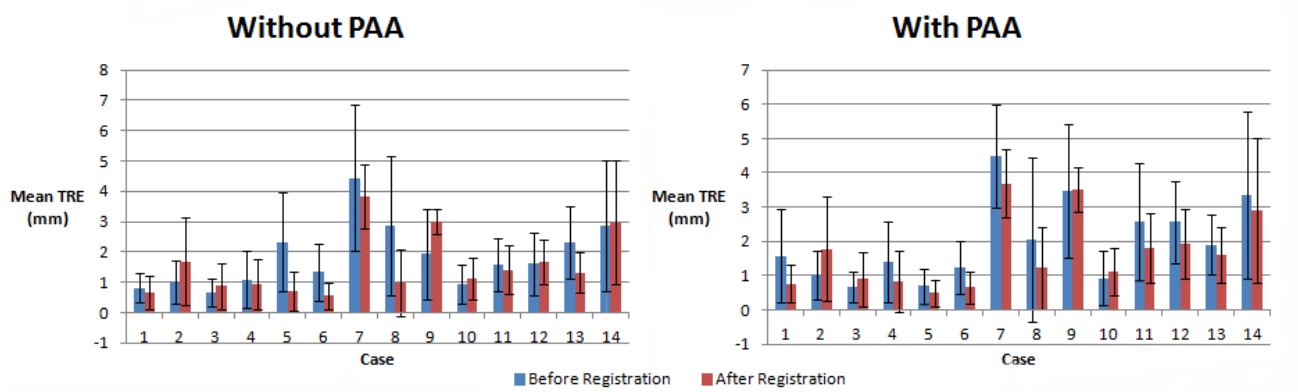

Figure 7: Mean target registration error for the fourteen cases before and after deformable registration. The whiskers denote the standard deviation. The principal axis alignment was not performed prior to the registration.

		Distance Driven	Pressure Driven
With PAA	**DSC**	0.97±0.01	0.95±0.02
	Mean TRE	1.8±1.7 mm	1.6±1.4 mm
	Volume Change	2.0±1.6%	1.5±1.4%
Without PAA	**DSC**	0.97±0.01	0.96±0.02
	Mean TRE	1.7±1.6 mm	1.5±1.4 mm
	Volume Change	1.7±1.4%	1.9±1.4%

Table 2: A comparison of the method of Ferrant et al.[16] (distance driven) and the method proposed in this paper (pressure driven) was performed by registering fourteen patient image sets using both methods. The results are shown in this table.

apex, around 2 mm near the base and 1 mm towards the center. In the latter, distances of 1.25 mm to 3.45 mm with an average of 2.36 mm were reported. Poor visibility of the urethra and the prostate boundary in the TRUS images is given as the reason for the higher error in the base and apex regions of the prostate. In our study, we saw values lower or equal to these results.

The main difference between our method and a similar method proposed before[10,11,16] is the computation of boundary conditions. Their method use gradient descent on a distance map to the target surface in order to determine external forces while our forces are driven by the global volume mis-alignment. As our technique is closest to the one employed by Ferrant et al.,[16] we performed registration for all the 14 cases using their method for comparison. We observed that the global volume mis-alignment allows the model to rotate more easily during the registration and leads to better matching within the interior. A comparison of the registration results for one case is shown in Figure 8. Using their method, we obtained a mean DSC of 0.97±0.01 both when PAA was not performed initially and when PAA was performed. We obtained a TRE of 1.7±1.6 mm when PAA was not performed and 1.8±1.7 mm when PAA was performed. The change in source surface volume was 1.7±1.4% when PAA was not performed and 2.0±1.6% when PAA was performed. As seen from these results (see table 2), although our method yields slightly lower DSC values, it in fact leads to lower TREs as an indication of better overall and internal registration, while also causing less volume change than this method used for comparison.

Based on our evaluation, the new registration technique presented in this paper is a promising tool for performing surface based registration. Perhaps its most promising aspect is the ability to combine the approach with elastography, so that the Young's modulus used in our registration can be the actual one obtained in-vivo in one or both of the imaging modalities.

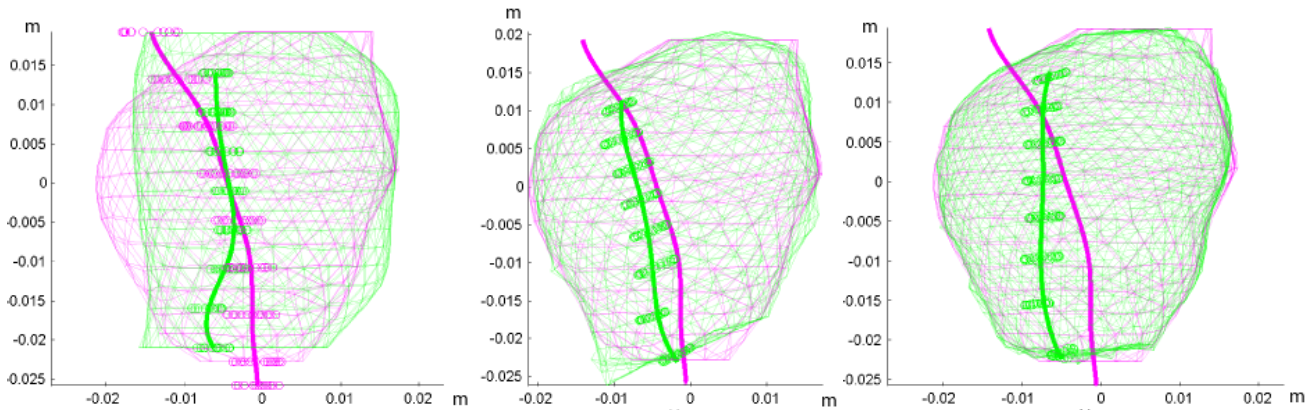

Figure 8: Case 9. The pink and green meshes represent the target and source surfaces respectively. The urethras from both the volumes are shown by the splines of the corresponding colours. (a) shows unregistered surfaces, (b) shows surfaces registered using our approach, and (c) shows surfaces registered using the approach by Ferrant et al.[16]

REFERENCES

[1] Singh, A., Kruecker, J., et al., "Initial clinical experience with real-time transrectal ultrasonography-magnetic resonance imaging fusion-guided prostate biopsy," *BJU international* **101**(7), 841–845 (2008).

[2] Reynier, C., Troccaz, J., Fourneret, P., Dusserre, A., Gay-Jeune, C., Descotes, J., Bolla, M., and Giraud, J., "MRI/TRUS data fusion for prostate brachytherapy. preliminary results," *Medical physics* **31**, 1568 (2004).

[3] Ling, C., Yorke, E., and Fuks, Z., "From IMRT to IGRT: frontierland or neverland?," *Radiotherapy and oncology* **78**(2), 119–122 (2006).

[4] Ukimura, O., Magi-Galluzzi, C., and Gill, I., "Real-time transrectal ultrasound guidance during laparoscopic radical prostatectomy: impact on surgical margins," *The Journal of urology* **175**(4), 1304–1310 (2006).

[5] Ten Haken, R., Forman, J., Heimburger, D., Gerhardsson, A., McShan, D., Perez-Tamayo, C., Schoeppel, S., and Lichter, A., "Treatment planning issues related to prostate movement in response to differential filling of the rectum and bladder," *International Journal of Radiation Oncology* Biology* Physics* **20**(6), 1317–1324 (1991).

[6] Shao, W., Wu, R., Thng, C., Ling, K., Ho, H., Cheng, C., and Ng, W., "Deformable registration for integration of MRI/MRSI information in trus-guided prostate biopsy," in [*Proceedings of SPIE*], **5747**, 1263 (2005).

[7] Mitra, J., Oliver, A., Marti, R., Lladó, X., Vilanova, J., and Meriaudeau, F., "Multimodal prostate registration using thin-plate splines from automatic correspondences," in [*Digital Image Computing: Techniques and Applications (DICTA), 2010 International Conference on*], 587–592, IEEE (2010).

[8] Wu, X., Dibiase, S., Gullapalli, R., and Yu, C., "Deformable image registration for the use of magnetic resonance spectroscopy in prostate treatment planning," *International Journal of Radiation Oncology* Biology* Physics* **58**(5), 1577–1583 (2004).

[9] Xuan, J., Wang, Y., Adali, T., Zheng, Q., Hayes, W., Freedman, M., and Mun, S., "A deformable surface-spine model for 3-D surface registration," in [*Image Processing, 1997. Proceedings., International Conference on*], **3**, 236–239, IEEE (2002).

[10] Bharatha, A., Hirose, M., Hata, N., Warfield, S., Ferrant, M., Zou, K., Suarez-Santana, E., Ruiz-Alzola, J., D'Amico, A., Cormack, R., et al., "Evaluation of three-dimensional finite element-based deformable registration of pre-and intraoperative prostate imaging," *Medical Physics* **28**, 2551 (2001).

[11] Noe, K. and Sørensen, T., "Solid Mesh Registration for Radiotherapy Treatment Planning," *Biomedical Simulation* , 59–70 (2010).

[12] Hu, Y., Ahmed, H., Taylor, Z., Allen, C., Emberton, M., Hawkes, D., and Barratt, D., "MR to ultrasound registration for image-guided prostate interventions," *Medical Image Analysis* (2010).

[13] Hensel, J., Ménard, C., Chung, P., Milosevic, M., Kirilova, A., Moseley, J., Haider, M., and Brock, K., "Development of multiorgan finite element-based prostate deformation model enabling registration of endorectal coil magnetic resonance imaging for radiotherapy planning," *International Journal of Radiation Oncology* Biology* Physics* **68**(5), 1522–1528 (2007).

[14] Brock, K., Sharpe, M., Dawson, L., Kim, S., and Jaffray, D., "Accuracy of finite element model-based multi-organ deformable image registration," *Medical physics* **32**, 1647 (2005).

[15] Zienkewickz, O. C. and Taylor., R. L., [*The Finite Element Method*], McGraw Hill Book Co., New York, 4th edition (1987).

[16] Ferrant, M., Nabavi, A., Macq, B., Jolesz, F., Kikinis, R., and Warfield, S., "Registration of 3-D intraoperative MR images of the brain using a finite-element biomechanical model," *Medical Imaging, IEEE Transactions on* **20**(12), 1384–1397 (2002).

[17] Treece, G., Prager, R., Gee, A., and Berman, L., "Surface interpolation from sparse cross sections using region correspondence," *Medical Imaging, IEEE Transactions on* **19**(11), 1106–1114 (2000).

[18] Si, H., "TetGen, a quality tetrahedral mesh generator and three-dimensional delaunay triangulator.," tech. rep., Technical Report 9, WIAS, Berlin, Germany (2004).

[19] "CGAL, Computational Geometry Algorithms Library." http://www.cgal.org.

[20] Kemper, J., Sinkus, R., Lorenzen, J., Nolte-Ernsting, C., Stork, A., and Adam, G., "MR elastography of the prostate: Initial in-vivo application," in [*Rofo. Fortschritte auf dem Gebiet der Rontgenstrahlen und der bildgebenden Verfahren*], **176**(8), 1094–1099, Thieme (2004).

[21] Porter, B., Taylor, L., et al., "Histology and ultrasound fusion of excised prostate tissue using surface registration," in [*Ultrasonics Symposium, 2001 IEEE*], **2**, 1473–1476, IEEE (2002).